arXiv:1602.07834v1 [physics.comp-ph] 25 Feb 2016

Fluctuation capture in non-polar gases and liquids

D. G. Cocks, R. D. White
College of Science, Technology and Engineering,
James Cook University, Townsville 4810, Australia

We present a new model to identify natural fluctuations in fluids, allowing us to describe localization phenomena in the transport of electrons, positrons and positronium through non-polar fluids. The theory contains no free parameters and allows for the calculation of capture cross sections $\sigma_{\rm cap}(\epsilon)$ of light-particles in any non-polar fluid, required for non-equilibrium transport simulations. We postulate that localization occurs through large shallow traps before stable bound states are formed. Our results allow us to explain most of the experimental observations of changes in mobility and annihilation rates in the noble gases and liquids as well as make predictions for future experiments. Quantities which are currently inaccessible to experiment, such as positron mobilities, can be obtained from our theory. Unlike other theoretical approaches to localization, the outputs of our theory can be applied in non-equilibrium transport simulations and an extension to the determination of waiting time distributions for localized states is straight forward.

Introduction—The transport of light particles (i.e. electrons e^-, positrons e^+ or positronium Ps) through materials takes place in a wide range of systems, occurring in plasma research, medical imaging, particle therapy, organic solar cells and particle detectors. Until recently, it was typical for transport in dense fluids (i.e. liquids and dense gases) to be modeled using the same assumptions as dilute gases, including effects of the medium only through terms linear in the bulk density, neglecting correlations between the fluid particles and assuming independent collisions between the light and fluid particles. Improvements to traditional transport theory have made use of the seminal works by Cohen and Lekner [1] to partially address the structure of a dense fluid [2] which explain order of magnitude changes in observed drift velocities and negative-differential-conductivities with an applied electric field.

Correlations in a dense structured fluid also introduce new processes such as "bubble capture" [3, 4], whereby a light-particle (LP) strongly interacts with the surrounding fluid to form a stable bound state, analogous to the polaron of solid-state physics. These bound states consist of a reduction or enhancement of the local density surrounding the light-particle, leading to "bubbles" or "clusters", respectively. The combined fluid/light-particle object can possess an effective mass much greater than the quasi-free particles leading to modified transport coefficients and even fractional diffusion [5]. For e^+ and Ps, the change in density surrounding the particle leads to significant enhancements or reductions in the annihilation rate and hence the observed lifetime of the particles.

This paper presents a new model for fluctuation capture which can be applied to all non-polar fluids without resorting to empirical inputs. To the knowledge of the authors, this model is the first to produce energy-dependent capture cross sections $\sigma_{\rm cap}(\epsilon)$, along with details sufficient to calculate energy-dependent waiting-time distributions $\theta(\epsilon, t)$. This enables the inclusion of fluctuation capture into non-equilibrium ab initio transport simulations.

There have been many indirect experimental observations of fluctuation capture and we choose to focus here on experiments in the noble gases. For e^-, there have been observations of reduced mobility in dense helium and neon gases [6–8], as well as fractional diffusion in liquid neon [9], and suggestions of fluctuation capture in xenon [10]. For e^+ and Ps, significant changes in annihilation rates have been observed for helium, neon, argon and xenon [4, 11–16] beyond the linear dependence on density expected in the dilute gas phase. Ps bubbles, which dramatically increase the Ps lifetime, have also been observed through the use of ACAR measurements in argon, krypton and xenon [17, 18].

Many theoretical investigations into fluctuations have focused only on the equilibrium state of the dressed particle [3, 4, 19]. In this paper, we are interested in an inherently non-equilibrium and dynamical process. Some previous investigations for light particles out of equilibrium have looked at "cavities" or "voids" within fluids, considering the largest available volume with a total absence of atoms [9, 20–24]. Far less prevalent are investigations into mesoscopic fluctuations with a weak perturbation of the density profile [25–28]. We emphasize that our focus here is on fluctuation capture of a light particle and so do not address the formation of Ps, which is a complex process [24].

Despite these previous investigations, we believe that a significant omission remains in the literature for fluctuation capture. As the de Broglie wavelength of a thermalized LP can extend to over hundreds of average fluid particle separations, it is disconnected with the picture of a tight compact void which is of the order of a single spacing. Many of the theoretical studies referenced above either assume the light-particle is already in the void, or invoke a classical description of the particle, at odds with the quantum nature dictated by the energy and length scales of the system. Instead we believe that a larger mesoscopic scale fluctuation is necessary to describe the leading contributions to localization and the stable trapped state results from a contraction of these large-scale fluctuations rather than expansion of

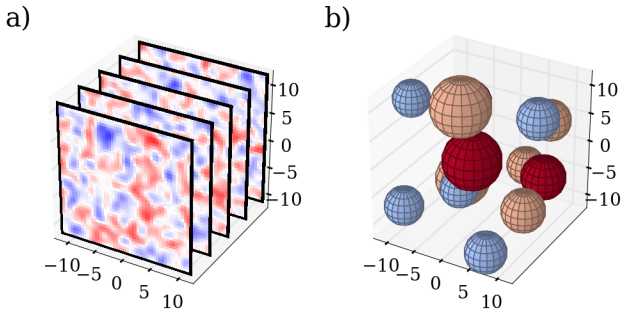

Figure 1. Steps in the fluctuation identification process for a single snapshot of a system with $T = 1.0\,T_{\mathrm{LJ}}$, $\rho = 0.71\,\rho_{\mathrm{LJ}}$. a) Cross-sections of the continuous density distribution obtained by Gaussian blurring the atomic positions. b) The identified fluctuations, represented as spheres whose radius is R_c and whose threshold t_c is given by the color, with blue (red) as the most deep (shallow) fluctuations.

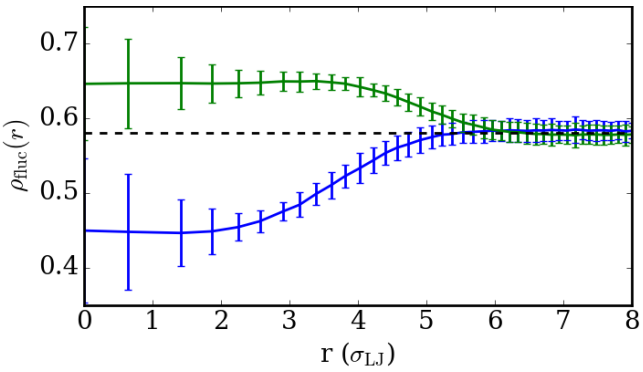

Figure 2. Mean density distributions, $\rho_{\mathrm{fluc}}(r)$ for a system with $T = 1.2T_{\mathrm{LJ}}$, $\rho = 0.58\rho_{\mathrm{LJ}}$ and a low-(high-)density fluctuation classified as $t_c = 0.84$, $R_c = 3.97$ ($t_c = 1.1$, $R_c = 4.99$) with one standard deviation in the statistical average shown. The large deviations for small r are expected, as these are sensitive to the exact positions of the atoms.

small-scale voids. Furthermore, we propose a general theory that can be applied to any material in the gas or liquid phases without requiring free parameters. We have applied this theory to the noble gases and liquids, successfully explaining almost all of the current experimental measurements and predict transport and localization behavior for combinations of atomic species and densities which have not yet been measured.

The energy-dependent capture cross-sections $\sigma_{\mathrm{cap}}(\epsilon)$ and waiting time distributions $\theta(\epsilon, \tau)$ obtained from this model can be used directly in solutions of the Boltzmann equation [5] and Monte-Carlo transport simulations. The inputs to our calculations are the fluid interparticle potential, the elastic cross sections for the light-particle/fluid interaction and certain hydrodynamic properties of the fluid. We choose to model the noble gases in their gaseous and liquid states by an untruncated Lennard-Jones (LJ) fluid with the appropriate values for the energy (ϵ_{LJ}) and length (σ_{LJ}) scales detailed in the supplementary material. The LJ parameters also provide a useful unit, $T_{\mathrm{LJ}} = \epsilon_{\mathrm{LJ}}/k_B$, for temperature. The calculation proceeds in four steps: identifying the fluctuations, calculating their properties, obtaining binding energies and calculating a rate of capture.

Fluctuation identification—It is first necessary to understand the distribution of fluctuations and their spatial profiles in the absence of the light particle, which we inevstigate by performing Monte-Carlo simulations of the LJ fluid, saving snapshots from the simulation. From these snapshots we create a continuous density distribution by blurring the atomic positions with Gaussians of width $\sigma_{\mathrm{blur}} = (3/4\pi\rho_0)^{1/3}$, corresponding to the Wigner-Seitz radius. An example of this blurred distribution is shown in figure 1a). We then take averages over the continuum density in spherical volumes throughout the fluid, gradually increasing the radii, R, of the volumes. A fluctuation will have an average density that deviates significantly from the bulk value even after averaging over a large region. For each averaging volume we look for connected regions with average densities that fall above or below a set of prescribed thresholds t_c. A high-(low-)density fluctuation is identified as the largest radius, R_c, that is above (below) the threshold for which a connected region can still be found. A sample of identified fluctuations is shown in figure 1b).

Fluctuation properties—For each fluctuation classified by the parameters $\{R_c, t_c\}$ we determine the density distribution spherically averaged about its center point, $\rho_{\mathrm{fluc}}^{\{R_c,t_c\}}(r)$ where r is the radial distance from the center of the fluctuation. To build up a good representation of a macroscopic liquid, we perform a statistical average over $\rho_{\mathrm{fluc}}^{(R_c,t_c)}(r)$ for many different uncorrelated snapshots of the Monte-Carlo simulation. We show some example density distributions, $\rho_{\mathrm{fluc}}^{(R_c,t_c)}(r)$, in figure 2. During the statistical averaging, we also extract a density of states for the fluctuations of the same threshold, $g_{t_c}(R_c)\,dR_c$, by binning the counts of the fluctuations into a coarse-grained grid of R_c.

The two quantities, $\rho_{\mathrm{fluc}}^{\{R_c,t_c\}}(r)$ and $g_{t_c}(R_c)$ are what sets this theory apart from others. These quantities are essential to allow the connection to macroscopic non-equilibrium transport simulations which require energy-resolved collision frequencies.

Binding energies and capture rate—We use the density profiles $\rho_{\mathrm{fluc}}^{(R_c,t_c)}(r)$ to calculate the probability that the fluctuation will capture an incoming light particle by performing a scattering calculation, whereby the initial quasi-free LP transitions to a bound state within the fluctuation, which requires us to define a scattering potential $V(r)$ and a coupling $W(\epsilon \to \epsilon_b)$. The effective interaction between the LP and the bulk, $V(r)$, is chosen in a homogeneous-energy local-density (HELD) approximation. The term "homogeneous energy" refers to the background energy felt by a quasi-free particle in a homogeneous system, $V_0(\rho_0)$, which has a complicated

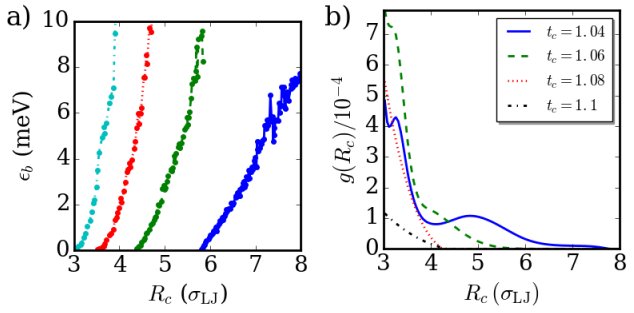

Figure 3. The a) binding energies, ϵ_b, and b) density of states, $g(R_c)$, for e^- within high-density fluctuations of argon at $T = 1.0\,T_{\rm LJ}$ and $\rho = 0.71\,\rho_{\rm LJ}$ for different identification thresholds t_c and as a function of fluctuation size R_c.

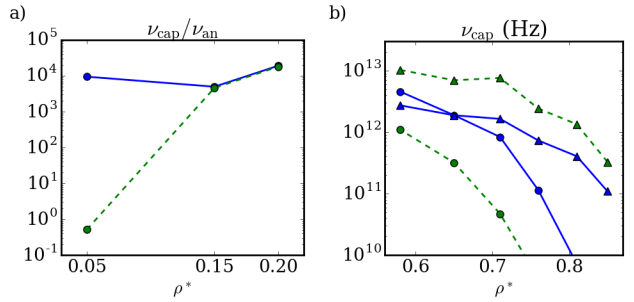

Figure 4. Thermally averaged capture rate $\nu_{\rm cap}$ for a) e^+ in the gas phase, and b) e^- and Ps in the liquid phase for argon (solid blue) and neon (dashed green). Ps curves are distinguished by triangular markers. The e^+ capture rate is compared to the annihilation rate $\nu_{\rm an}$.

non-linear dependence on bulk density [29]. We connect this to the effective interaction by assuming that the LP feels the local density only, i.e. $V(r) = V_0(\rho(r))$. This "local approximation" neglects effects from the spatial-dependence of screening (note, however, that non-local effest of microscopic screening are included within V_0) which is negligible for the small density changes we consider, and has fared very well in previous calculations [29]. The sign of V_0 determines the types of fluctuations that are favored by the light particle: low-density bubbles or high-density clusters for $V_0 > 0$ and $V_0 < 0$ respectively.

In this paper, we choose a simple representation of V_0 for the sake of clarity. Instead of the full non-linear dependence, we take $V_0(\rho_0) \approx 2\pi\hbar^2 a_s \rho_0/m$ where the scattering length a_s describes a Born-like approximation for the LP-atom interaction. We emphasize that we make this choice only so that we may easily present our results for a range of different atomic species, and it is trivial to to apply a more accurate form of $V_0(\rho)$ given the appropriate data from theory [29] or experiment [30].

For Ps we also include an additional term [31] in the local potential $V_{ps}(\boldsymbol{r}) = V_0(\rho(\boldsymbol{r})) - V_\epsilon(\rho(\boldsymbol{r}))$ where $V_\epsilon = \frac{E^0_{ps}}{\epsilon_r^2}$, $E^0_{ps} = 13.6\,\text{eV}/4$ is the binding energy of Ps in vacuum and $\epsilon_r = \epsilon_r^\infty(\rho)$ is the high-frequency relative permittivity of the fluid.

Performing an s-wave scattering calculation with the local potential $V(r)$ results in scattering wavefunctions $\psi_{\rm sc}(r)$ and bound states $\psi_b(r)$ with binding energies ϵ_b, shown in figure 3 a). We note that, at these energies, higher partial waves do not contribute as the centrifugal energy at the edge of the bubble $\hbar^2/2mR_c^2 \geq 20\,\text{meV}$ is comparable to the thermal energy, and only low energy LPs are strongly coupled to the bound states. To confirm this, we have calculated the p-wave contribution for capture of e^-, e^+ and Ps in argon and found it to be less than 1% of the s-wave contribution. The same arguments also apply for bound states with $l \geq 1$.

The coupling between the scattering and bound state which depends spatially on the LP wavefunction and fluid density. We consider scattering of the LP from sound mode phonons that provide the necessary transfer of energy and momentum for capture into the fluctuations. As we show in the supplementary material [], attaining the appropriate transition rate from quasi-free to bound states using Fermi's golden rule results in a capture rate given by

$$W(\epsilon \to \epsilon_b) = \frac{S(0)}{4}\sqrt{\frac{2}{m}}\int dr\,\psi_\epsilon(r) j_0(\Delta k\, r)\psi_{\epsilon_b}(r) \times\rho(r)\sqrt{\tilde{\epsilon}}\sigma_{\rm atom}(\tilde{\epsilon}). \quad (1)$$

where $j_l(x)$ is the regular spherical Bessel function, $\tilde{\epsilon} = \max(\epsilon - \tilde{V}(r), 0)$ and $\Delta k = c_s|\Delta\epsilon|$ where c_s is the speed of sound. Equation (1) can be roughly understood as an overlap integral between the scattering and bound states, $\psi_\epsilon(r)$ and $\psi_{\epsilon_b}(r)$ respectively, where momentum Δk is transferred corresponding to the sound mode dispersion relation and the coupling is dependent on the local cross-section for a collision producing a sound wave, $\frac{S(0)}{4}\sqrt{\tilde{\epsilon}}\sigma_{\rm atom}(\tilde{\epsilon})$, as well as the local atomic density, $\rho(r)$. Due to conservation of momentum and energy, only low-energy LPs can be captured by the flucutation.

The transition rate, $W(\epsilon \to \epsilon_b)$ defines a cross-section for capture $\sigma_{\rm cap}^{\{R_c,t_c\}}(\epsilon)$ in a collision with a single fluctuation. The overall capture rate, expressed as a collision frequency, is then found by integrating over the density of states for all available fluctuations:

$$\nu_{\rm cap}(\epsilon) = \sqrt{\frac{2\epsilon}{m}}\sum_{t_c}\int dR_c\,\sigma_{\rm cap}^{\{R_c,t_c\}}(\epsilon) g_{t_c}(R_c). \quad (2)$$

Results in the noble gases and liquids—We determine the fluctuation properties $\rho_{\rm fluc}^{(R_c,t_c)}(r)$ and $g_{t_c}(R_c)$ and perform the integrations (1) and (2) using LJ parameters for neon, argon, krypton and xenon. Six points on the liquid side of the gas-liquid coexistence region, spanning $0.58 \leq \rho_{\rm LJ} \leq 0.85$ were chosen, as well as three points in the gas phase, spanning $0.05 \leq \rho_{\rm LJ} \leq 0.20$ at

		$\nu_{\rm cap}^{\rm th}$ ($\times 10^{12}$ Hz)	Exp ($\rho\uparrow$)	Ref	Agreement
e^-	Ne	EI zero $\to 1$	$\mu\downarrow$, $\rho_{\rm LJ}\gtrsim 0.20$	[32]	Possible
	Xe	AL $1 \to 10$	$\mu\downarrow$, all $\rho_{\rm LJ}$	[10]	Good
		$\nu_{\rm cap}/\nu_{\rm an}$			
e^+	Ar	AL $\approx 10^3$	$Z_{\rm eff}\uparrow$, all $\rho_{\rm LJ}$	[33]	Good
	Ne	EI zero $\to 10^4$	$Z_{\rm eff}$ const	[12]	Good*
	Xe	AL $\approx 10^2$	$Z_{\rm eff}\uparrow$, $\rho_{\rm LJ}\to 0$	[16]	Good
Ps	Ar	EI $10^4 \to 10^5$	$Z_{\rm eff}^1\downarrow$	[33]	Good
	Ne	EI $10^4 \to 10^6$	$Z_{\rm eff}^1\downarrow$, $\rho_{\rm LJ}\gtrsim 0.10$	[12]	Good*
	Kr	EI $10^4 \to 10^5$	N/A		
	Xe	EI $10^3 \to 10^4$	$Z_{\rm eff}^1\downarrow$, $\rho_{\rm LJ}\gtrsim 0.15$	[16]	Good*

Table I. Comparison of thermally averaged $\nu_{\rm cap}^{\rm th}$ to experiments in dense gases. For e^-, a baseline of $\nu_{\rm cap} = 10^{12}$ Hz is used, see main text for details, and is compared to the experimental mobility μ. For e^+ and Ps, $\nu_{\rm cap}$ is compared to direct annihilation $\nu_{\rm an}$. Shorthand notation of EI (exponential increase) and AL (always large) have been used to qualitatively describe the theoretical results. The trend of the experimental observations is indicated for increasing density as the gas approaches the gas-liquid phase transition or the critical density. An asterisk indicates that time evolution of the fluctuation is required to explain the good agreement.

		$\nu_{\rm cap}^{\rm th}$ ($\times 10^{12}$ Hz)	Exp ($\rho\downarrow$)	Ref	Agreement
e^-	Ne	EI zero $\to 1$	SM near CP	[9]	Good
	Xe	AL $1 \to 10$	$\mu\uparrow$	[10]	Possible
		$\nu_{\rm cap}/\nu_{\rm an}$			
e^+	Ar	AL $\approx 10^4$	$Z_{\rm eff}$ constant	[33]	Bad
	Ne	Only $T^* = 1.2$	N/A		N/A
	Xe	Const ≈ 1	$Z_{\rm eff}$ constant	[16]	Good
Ps	Ar	EI $10^3 \to 10^4$	$Z_{\rm eff}^1\downarrow$	[33]	Good
	Ne	EI $10^3 \to 10^4$	Bubbles in ACAR	[17]	Good
	Kr	EI $10^3 \to 10^4$	Bubbles in ACAR	[17]	Good
	Xe	EI $10^1 \to 10^3$	$Z_{\rm eff}^1\downarrow$	[16]	Good

Table II. Summary of results with comparison to liquid experiments. Details are as table I. Note, however, that the experimental trend is given as density *decreases* towards the gas-liquid phase transition or critical density. The shorthand "SM near CP" stands for "Scher-Montroll behavior near the critical point".

constant temperature $T_{\rm LJ} = 1.3$. Note that the critical temperature and density for the untruncated LJ fluid are $\rho_{{\rm LJ},c} \approx 0.3$ and $T_{{\rm LJ},c} \approx 1.33$. We used the static structure factor $S(0)$ calculated from the pair correlator of our Monte-Carlo simulations for each temperature and density.

As shown in tables I and II, our results agree favorably with most of the experimental data we have found. This is remarkable, given the gas scattering-length approximation we have made for V_0. In general, we try to compare the thermally averaged capture rate, $\nu_{\rm cap}^{\rm th}$, to relevant time scales of the transport. For e^+ and Ps this is naturally represented by its ratio to the annihilation frequency $\nu_{\rm an}$, as capture must be fast enough to observe an increase in total annihilation rate, more commonly described as an increase in the effective electron number per atom, $Z_{\rm eff}$ and $Z_{\rm eff}^1$ for e^+ and Ps respectively.

For e^- a natural time scale for comparison is the transit time, which is unfortunately different for each experimental configuration. However, we have found that assuming noticeable capture frequencies must be 10^{12} Hz or larger gives very good agreement with experimental observations (an improved comparison requires a full transport calculation). In neon, we predict that as the density in the gas (liquid) phase is increased (decreased), capture becomes exponentially more likely. This follows the observation of "activation" densities in experiment, where modified mobilities μ [32] or Scher-Montroll behavior [9] occur for a limited range of densities about the critical point. For xenon, we predict a strong capture rate for all of the densities we investigated, which agrees well for experiments in the gas phase [10]. In the liquid phase there is possible agreement, but the experimental observations are overwhelmed by an increase in mobility which is likely due to a non-linear change of V_0 to repulsive behavior [30], neglected in our scattering length approximation.

For e^+ in gases, our predictions of strong capture rates agree well with experiments in argon [33] and xenon [16]. In contrast, experiments in neon [12] see no increased annihilation which appear to contradict our results. However, this can be explained through preliminary calculations of the Navier-Stokes evolution of the high-density fluctuation into a cluster, see supplementary material []. Because the e^+-Ne interaction is weak in comparison to the other noble gases, the bound state is quickly lost in time evolution before a significant change in fluid density can occur. In the liquid phase, we find agreement with xenon measurements, whereby a capture rate is obtained that is too slow to modify the total annihilation rate. Unfortunately, our prediction of a strong capture rate in argon liquid is at odds with experimental observations [33] and is not easily explained through our preliminary time evolution calculations. We conjecture that non-linearities in V_0 play a dominant role in this case.

In general, Ps has been observed to form bubbles in all noble-gas liquids [16, 17, 33] and for high-density gases [12], in agreement with our calculations. However, our results also predict that strong capture rates persist even to relatively dilute gases. The apparent discrepancy can easily be explained by identifying the wide and shallow profiles corresponding to these fluctuations, which do not allow the formation of stable bubbles in the subsequent time-evolution.

Conclusion—We have developed a theory, valid in

both dense gases and liquids, which describes scattering of light particles into large-scale natural fluctuations and the formation of trapped states. The theory has no fitting parameters and agrees well with almost all of the experimental literature in the noble gases and liquids. This work represents the first calculation of $\sigma_{\rm cap}(\epsilon)$ which will be used in upcoming transport calculations that are far from equilibrium, combined with a model of the time-dependence of the fluctuations that describes the waiting time distribution for the localized states [5, 34]. The strongest approximation in the calculations presented here is the use of a gas scattering-length which can be improved by considering Wigner-Seitz models [30]. Further investigations will also be extended to include non-local contributions (e.g. including spatial dependence of screening) which would also provide a natural pathway to describing polar molecules.

[1] M. Cohen and J. Lekner, Phys. Rev. **158**, 305 (1967).
[2] G. J. Boyle, R. P. McEachran, D. G. Cocks, and R. D. White, J. Chem. Phys. **142** (2015), 10.1063/1.4917258.
[3] I. T. Iakubov and A. G. Khrapak, **45**, 697 (1982).
[4] J. Hernandez, Reviews of Modern Physics **63**, 675 (1991).
[5] B. Philippa, R. E. Robson, and R. D. White, New J. Phys. **16**, 073040 (2014).
[6] A. Bartels, **64**, 59 (1975).
[7] J. a. Jahnke and M. Silver, Chem. Phys. Lett. **19**, 231 (1973).
[8] A. Borghesani and M. Santini, Phys. Rev. A **45**, 8803 (1992).
[9] Y. Sakai, W. F. Schmidt, and A. Khrapak, Chem. Phys. **164**, 139 (1992).
[10] S. S.-S. Huang and G. R. Freeman, J. Chem. Phys. **68**, 1355 (1978).
[11] K. Canter, J. McNutt, and L. Roellig, Phys. Rev. A **12**, 375 (1975).
[12] K. Canter and L. Roellig, Phys. Rev. A **12**, 386 (1975).
[13] K. Rytsola, J. Vettenranta, and P. Hautojarvi, J. Phys. B: At. Mol. Phys. **17**, 3359 (1984).
[14] I. Pepe, D. A. L. Paul, J. Steyaert, F. Gimeno-Nogues, J. Deutsch, and R. Prieels, J. Phys. B: At. Mol. Opt. Phys. **28**, 3643 (1995).
[15] R. Nieminen, I. Välimaa, M. Manninen, and P. Hautojärvi, Phys. Rev. A **21**, 1677 (1980).
[16] M. Tuomisaari, K. Rytsola, and P. Hautojarvi, J. Phys. B: At. Mol. Opt. Phys. **21**, 3917 (1999).
[17] P. G. Varlashkin, Phys. Rev. A **3**, 1230 (1971).
[18] P. G. Coleman, S. Rayner, F. M. Jacobsen, M. Charlton, and R. N. West, J. Phys. B: At. Mol. Opt. Phys. **27**, 981 (1999).
[19] B. N. Miller and T. Reese, Nuclear Instruments and Methods in Physics Research Section B: Beam Interactions with Materials and Atoms **192**, 176 (2002).
[20] K. V. Mikhin, S. V. Stepanov, and V. M. Byakov, High Energy Chemistry **39**, 36 (2005).
[21] J. Schnitker, P. J. Rossky, and G. a. Kenney-Wallace, J. Chem. Phys. **85**, 2986 (1986).
[22] A. Vishnyakov, P. G. Debenedetti, and A. V. Neimark, Phys. Rev. E **62**, 538 (2000).
[23] V. K. Shen and P. G. Debenedetti, J. Chem. Phys. **111**, 3581 (1999).
[24] S. V. Stepanov, V. M. Byakov, D. S. Zvezhinskiy, G. Duplâtre, R. R. Nurmukhametov, and P. S. Stepanov, Advances in Physical Chemistry **2012**, 1 (2012).
[25] T. P. Eggarter and M. H. Cohen, Phys. Rev. Letters **27**, 129 (1971).
[26] B. Space and D. Coker, J. Chem. Phys. **96**, 652 (1992).
[27] T. Truskett, S. Torquato, and P. Debenedetti, Phys. Rev. E **58**, 7369 (1998).
[28] N. J. English and J. S. Tse, Phys. Rev. Letters **106**, 037801 (2011).
[29] S. Nazin and V. Shikin, Physical Review Letters **101**, 166406 (2008).
[30] C. M. Evans and G. L. Findley, Physical Review A **72**, 022717 (2005).
[31] S. V. Stepanov and V. M. Byakov, The Journal of Chemical Physics **116**, 6178 (2002), arXiv:0209105 [physics].
[32] A. Borghesani and M. Santini, Phys. Rev. A **42**, 7377 (1990).
[33] M. Tuomisaari, K. Rytsölä, and P. Hautojärvi, Physics Letters A **112**, 279 (1985).
[34] P. W. Stokes, B. Philippa, D. Cocks, and R. D. White, (2015), arXiv:1510.01632.
[35] R. Ramírez and C. P. Herrero, Journal of Chemical Physics **129**, 1 (2008), arXiv:1109.1126.
[36] *Tables of Physical & Chemical Constants*, 16th ed. (Kaye & Laby Online (2005), 1995).
[37] W. Martienssen, Y. Itikawa, S. Buckman, J. Cooper, M. Elford, M. Inokuti, and H. Tawara, "Electron collisions with atoms," in *Landolt-Börnstein: Photon and Electron Ineractions with Atoms, Molecules and Ions.*, Landolt-Börnstein Photon and Electron Ineractions with Atoms, Molecules and Ions., Vol. 17 (Springer Verlag, 1997) Chap. 2, pp. 2–67.
[38] D. G. Green, J. a. Ludlow, and G. F. Gribakin, Phys. Rev. A **90**, 032712 (2014), arXiv:1404.5243.
[39] J. Mitroy and M. Bromley, Phys. Rev. A **67**, 1 (2003).
[40] L. Wang, *Three-body effects on the phase behaviour of noble gases from molecular simulation*, Ph.D. thesis, Swinburne University of Technology (2005).
[41] D. R. Lide, ed., *CRC Handbook of Chemistry and Physics*, 85th ed. (CRC Press, 2004).
[42] I. I. Fabrikant and G. F. Gribakin, , 3 (2014).
[43] R. L. Amey and R. H. Cole, J. Chem. Phys. **40**, 146 (1964).
[44] V. A. Rabinovich, V. I. Nedostup, T. Selover, A. A. Vasserman, and L. S. Veksler, *Thermophysical properties of neon, argon, krypton and xenon* (Springer, Berlin, 1988).
[45] J. Hoshen and R. Kopelman, Phys. Rev. B **14**, 3438 (1976).
[46] J. P. Hansen and I. R. McDonald, *Theory of Simple Liquids* (1976).
[47] K. Meier, A. Laesecke, and S. Kabelac, **3671** (2012), 10.1063/1.1770695.

Atom	ϵ_{LJ} (k_B/K)	r_{LJ} (Å)	c_s m/s	e^- a_s (a_0)	e^+ a_s (a_0)	Ps a_s (a_0)	K_{CM} (cm^3/mole)
Ne	37.29 [35]	2.782	540 [36]	0.215 [37]	−0.467 [38]	1.56 [39]	2.290
Ar	119.8 [40]	3.405	813 [41]	−1.452 [37]	−4.41 [38]	2.14 [42]	4.106 [43]
Kr	164.4 [40]	3.638	1120 [44]	−3.35 [37]	−9.71 [38]	2.35 [42]	6.239 [43]
Xe	231.1 [40]	3.961	1090 [44]	−6.3 [37]	−84.5 [38]	2.29 [39]	9.685 [43]

Table III. Parameters used for each of the noble gas species in the calculations. K_{CM} is the Claussius-Mossotti coefficient, defined by $\epsilon_r(\rho) = \frac{1+2K_{CM}\rho}{1-K_{CM}\rho}$. The LJ parameters for argon, krypton and xenon have been taken from the "Horton" values listed in [40]. <Citations for all numbers!>

Appendix A: Details of Fluctuation Identification

We include some additional details of the identification procedure here. As described in the main text, the identification of fluctuations occurs by 1) Gaussian blurring, 2) classification of fluctuations identified by an average in a spherical volume of radius R_c less than a threshold t_c, 3) obtaining the density distribution for each fluctuation.

The Gaussian blurring is done through representing a continuum density distribution on a fine grid, replacing each discrete atom by a Gaussian of width $\sigma_{\text{blur}} = (3/4\pi\rho_0)^{1/3}$:

$$\rho(\boldsymbol{x}) = \sum_{i=0}^{N} \frac{1}{(2\pi\sigma_{\text{blur}}^2)^{3/2}} e^{-|\boldsymbol{x}_i - \boldsymbol{x}|_L^2/2\sigma_{\text{blur}}^2} \tag{A1}$$

where $|\dots|_L$ indicates the smallest separation between the two points accounting for periodic boundaries. We make sure that each atom is individually normalized on the grid before adding it to the total density distribution.

Next, the density distribution is averaged in a sphere of radius R_c around each grid point. The radii are taken to be successively larger and, when searching for bubbles, we choose to identify these regions as connected groups of grid points whose average in a radius R_c is smaller than a given threshold t_c relative to the homogeneous density, ρ_0, i.e. $\rho_{\text{avg}} < t_c\rho_0$. These groups are identified using the Hoshen-Kopelman cluster-identification algorithm [45]. The process is identical for high-density fluctuations except that the condition is for the average to be larger than the given threshold t_c, i.e. $\rho_{\text{avg}} > t_c\rho_0$. For thresholds close to unity or for small radii, there may be many connected groups that span a large number of grid points. For example, a weak threshold $t_c = 1.0001$ would likely identify a group of points which percolate across the entire system. However, as the threshold or the radius is increased, each connected group becomes smaller and more defined until the point at which it disappears. As we only wish to identify the location of the group itself, we look for these points where a group disappears on increase of R_c or t_c. Practically this is done by filtering out overlapping fluctuations from a sequence of identifications done for different R_c values at a fixed threshold.

We are only interested in fluctuations that are larger than the average spacing between molecules, so we begin the R_c scan at $R_{c,\min} = 3$. The identification process should be reasonably insensitive to the choice of $R_{c,\min}$, so long as it remains small enough to allow for the larger fluctuations of interest. Changes in $R_{c,\min}$ should be reflected as changes in the t_c assigned to each fluctuation.

The location for each fluctuation identified in this manner can be taken to be the center of the group of grid points, found through the mean position of all grid points in the group. For periodic systems, such a mean can be ambiguous (e.g. when the group spans a boundary of the system) however our case is much simpler, as each group is comprised of only a few connected points. Practically, we identify the fluctuation position as the grid point in the group which minimizes the sum of distances to all other grid points in the group.

Appendix B: Capture Coupling Strength

The capture cross section described in the main text results from a coupling between the incoming scattering state and a bound state in the fluctuation. We use Fermi's golden rule to obtain an approximate coupling and fix the prefactor by a free-to-free scattering event. We assume the coupling itself is a result of the collision of the incoming light-particle with a sound mode, which is necessary to produce the energy transfer required. Hence, we postulate that the time-dependent coupling in a homogeneous fluid is of the form

$$V_{\text{coup}}(\boldsymbol{x}, t) = C(\Delta\epsilon) e^{i(\Delta\boldsymbol{k}\cdot\boldsymbol{x} - \Delta\epsilon t/\hbar)}. \tag{B1}$$

The function $C(\Delta\epsilon)$ can be found by comparing to a free-to-free scattering event with that of the Boltzmann equation, resulting in:

$$C_{\text{homo}}(\Delta\epsilon) = \rho_0 \sqrt{\frac{2}{m}} \int d\Delta k\, \sigma_{\text{sound}}(\Delta k, \Delta\epsilon). \tag{B2}$$

The cross section for a collision with a sound mode, $\sigma_{\text{sound}}(\Delta k, \Delta\epsilon)$, is approximated for small energy transfer by its form in the hydrodynamic limit [46] and neglecting sound wave attenuation, $\sigma_{\text{sound}}(\Delta k, \Delta\epsilon) \approx \frac{1}{4} S(0)\delta(\Delta\epsilon + c_s\Delta k)\sigma_{\text{atom}}(\epsilon)$. Here, $\sigma_{\text{atom}}(\epsilon)$ is the atomic cross-section which we approximate at these low energies by$\sigma_{\text{atom}} = 4\pi a_s^2$ where a_s is the scattering length, with the explicit values used listed in table III.

The factor of 1/4 arises from our interest in only the creation of sound modes and not collisions from existing sound waves, as well as assuming the adiabatic ratio is $\gamma \approx 2$. This leaves us with:

$$C_{\text{homo}}(\Delta\epsilon) = \frac{\hbar}{2\pi}\frac{S(0)}{4}\sqrt{\frac{2}{m}}\rho_0\sqrt{\epsilon}\sigma_{\text{atom}}(\epsilon). \tag{B3}$$

In the non-homogeneous case of a fluctuation, we make a simple local approximation to the velocity, substituting $\epsilon \to \tilde{\epsilon} = \max(\epsilon - \tilde{V}(r), 0)$, resulting in:

$$C(\Delta\epsilon) = \frac{\hbar}{2\pi}\frac{S(0)}{4}\sqrt{\frac{2}{m}}\rho(\boldsymbol{r})\sqrt{\tilde{\epsilon}}\sigma_{\text{atom}}(\tilde{\epsilon}). \tag{B4}$$

Finally, substituting (B4) and (B1) into Fermi's golden rule, and then integrating over angles results in equation (1).

Appendix C: Preliminary Time Evolution Results

To investigate the time-dependent behavior of the fluctuation after capture of the light particle, we perform a crude hydrodynamic evolution of the fluid density using the Navier-Stokes equations. Although the stable bubble or cluster is a microscopic system, where the validity of hydrodynamic limit is highly questionable, we are mostly interested in the initial behavior of the fluctuation which is at a mesoscopic scale.

The Navier-Stokes equations we use assume spherical symmetry and hence take the form:

$$\frac{\partial\rho}{\partial t} = -\frac{1}{r^2}\frac{\partial}{\partial r}\left(r^2\rho(r,t)u(r,t)\right) \tag{C1}$$

$$\begin{aligned}\frac{\partial u}{\partial t} + u\frac{\partial u}{\partial r} =& -\frac{\nabla P(\rho)}{\rho} + \frac{\nu(\rho)}{\rho}\frac{\partial}{\partial r}\left(r^2\frac{\partial u}{\partial r}\right) \\ &+ \frac{1}{3}\nu\nabla(\frac{1}{r^2}\frac{\partial(r^2u)}{\partial r^2}) - \frac{\nabla V(\rho,\psi)}{\rho}\end{aligned} \tag{C2}$$

where $u(r,t)$ is the flow velocity, $P(\rho)$ is the local pressure obtained from our Monte-Carlo simulations at varying densities and $\nu(\rho)$ is the viscosity given for the LJ fluid in [47]. The force on the fluid results from the potential V, which depends on the fluid/light-particle interaction given by $V(\rho,\psi) = V_0(\rho)|\psi|^2$ where V_0 is defined in the main text.

We assume the wavefunction adiabatically follows the fluid density profile and so integrate equations (C1) and (C2) in time, regularly recalculating the wavefunction after small time intervals. We continue the integration until either the binding energy of the light particle stabilizes, indicating a stable dressed particle has been reached, or until the profile no longer supports a bound state, in which case the light particle has been "popped" from the fluctuation and is assumed to return to a quasi-free state.

We note that a simple estimate of the stability of the bubble in the dilute gas limit can be obtained by comparing the forces due to pressure and the light-particle interaction. As $P \propto \rho$ and $V_0(\rho) \propto \rho$ for dilute gases and the wavefunction density decreases with size of fluctuation $|\psi|^2 \propto 1/R_c$, then the ratio $V/P \propto 1/R_c$. This means that the fluid/light-particle interaction becomes less important the larger the fluctuations and hence the more dilute the gas.